



# The mechanical and thermal setup of the GLORIA spectrometer

C. Piesch<sup>1</sup>, C. Sartorius<sup>1</sup>, F. Friedl-Vallon<sup>1</sup>, T. Gulde<sup>1</sup>, S. Heger<sup>1</sup>, E. Kretschmer<sup>1</sup>, G. Maucher<sup>1</sup>, H. Nordmeyer<sup>1</sup>, J. Barthel<sup>2</sup>, A. Ebersoldt<sup>3</sup>, F. Graf<sup>1,\*</sup>, F. Hase<sup>1</sup>, A. Kleinert<sup>1</sup>, T. Neubert<sup>4</sup>, and H. J. Schillings<sup>5</sup>

<sup>1</sup>Institut für Meteorologie und Klimaforschung, Karlsruher Institut für Technologie, Karlsruhe, Germany

<sup>2</sup>Institut für Energie und Klimaforschung – Stratosphäre, Forschungszentrum Jülich, Jülich, Germany

<sup>3</sup>Institut für Prozessdatenverarbeitung und Elektronik, Karlsruher Institut für Technologie, Karlsruhe, Germany

<sup>4</sup>Zentralinstitut für Engineering, Elektronik und Analytik – Systeme der Elektronik, Forschungszentrum Jülich, Jülich, Germany

<sup>5</sup>Zentralinstitut für Engineering, Elektronik und Analytik – Engineering und Technologie, Forschungszentrum Jülich, Jülich, Germany

\* now at: Deutsches SOFIA Institut, Universität Stuttgart, Stuttgart, Germany

Correspondence to: C. Piesch (christof.piesch@kit.edu)

Received: 2 October 2014 – Published in Atmos. Meas. Tech. Discuss.: 6 November 2014

Revised: 13 February 2015 – Accepted: 24 February 2015 – Published: 16 April 2015

**Abstract.** The novel airborne Gimballed Limb Observer for Radiance Imaging of the Atmosphere (GLORIA) measures infrared emission of atmospheric trace constituents. GLORIA comprises a cooled imaging Fourier transform spectrometer, which is operated in unpressurized aircraft compartments at ambient temperature. The whole spectrometer is pointed by the gimbal towards the atmospheric target. In order to reach the required sensitivity for atmospheric emission measurements, the spectrometer optics needs to operate at a temperature below 220 K. A lightweight and compact design is mandatory due to limited space and high agility requirements. The cooled optical system needs to withstand high pressure and temperature gradients, humidity, and vibrations. A new cooling system based on carbon dioxide and liquid nitrogen combined with high-performance insulation has been developed to meet the mechanical, thermal, and logistical demands. The challenging mechanical and spatial requirements lead to the development of a novel rigid linear slide design in order to achieve the large optical path difference for high spectral resolution. This paper describes the mechanical and thermal setup of GLORIA and presents the performance results on two different research aircrafts.

## 1 Introduction

The Gimballed Limb Observer for Radiance Imaging of the Atmosphere (GLORIA; Friedl-Vallon et al., 2014) is a cooled Fourier transform infrared (FTIR) spectrometer which has been designed to fly on board the German research aircraft HALO (Krautstrunk and Giez, 2012) or the Russian M55 Geophysica (Myasichev Design Bureau (MDB), 2002). It measures the infrared emission of atmospheric species in the spectral range from 780 to 1400 cm<sup>-1</sup>. For this purpose, the scene is observed through a Michelson linear-slide interferometer and imaged on a detector focal plane array (FPA).

Low temperature operation, as already proven in the previous balloon and aircraft borne spectrometers SIRIS (Brasunas et al., 1988), MIPAS-B2 (Friedl-Vallon et al., 2004), MIPAS-STR (Piesch et al., 1996) and CRISTA-NF (Kullmann et al., 2004), enables the detection of the characteristic infrared emission spectral features of atmospheric species at good signal to noise ratio.

The spectrometer is mounted in a three-axis gimbal to provide pointing stability and agility to enable different atmospheric observation modes (Friedl-Vallon et al., 2014): in chemistry mode (CM) with high spectral resolution, the line of sight is nearly perpendicular to the flight direction; whereas in dynamics mode (DM) with high spatial resolution, the instrument scans the horizon stepwise with gimbal yaw angle ranging from 45 to 132°, performing tomographic

measurements. The agility of the gimbal also allows nadir measurements and deep space calibration as well as pointing towards the blackbody calibration system (Olschewski et al., 2013).

The instrument is operated in unpressurized compartments and observes the atmospheric radiation through an opening on the side of the instrument bay. An installation in the pressurized cabin would require a window outside the calibration path of the instrument. Consequently, the instrument is exposed to the air flow and to variable ambient conditions depending on the flight profile, the aircraft velocity, and the meteorological situation. Overall instrument operation reliability and performance are influenced by environmental parameters such as temperature, humidity, vibration and pressure. A high-speed data acquisition system collects the scientific data as well as a large number of housekeeping data including the ambient conditions and the status of the GLORIA instrument.

The gimballed movement of the instrument requires a lightweight and compact mechanical design of the spectrometer which incorporates an integrated cooling system. In addition, a mechanically rigid structure for the sensitive optics of the interferometer is necessary in order to gain robustness against vibrations which are stimulated aerodynamically at the opening of the instrument bay and by the aircraft itself. The cooling system has to meet the needs of campaign operation with long flights and short stopovers at airports with limited infrastructure.

Section 2 describes the mechanical and thermal requirements of the airborne GLORIA spectrometer. The selected concept and its implementation are presented. The efforts which were made to achieve a stiff and thermally insulated optic module are emphasized. Furthermore the dedicated cooling system and its operation are shown. Sect. 3 follows a description of the environmental conditions during flights on both the M55 Geophysica aircraft and the G550 HALO aircraft based on sensor data. Finally the performance of the mechanical and thermal system is discussed in Sect. 4.

## 2 Mechanical and thermal design

### 2.1 Requirements

The mechanical structure of the spectrometer houses the optical components comprising a 9 cm double sided optical path difference Michelson interferometer and an infrared detector unit which accepts an incoming beam with a nominal diameter of 36.1 mm and a maximal divergence of 4.1 by 4.1°. Out of the possible configurations for Fourier transform spectrometers (Carli et al., 1999), a single linear-slide two-port configuration with cube corners was selected for compactness, robustness, and optical (vignetting) considerations. This optical setup is not shear-compensated and requires alignment. Since the instrument is operated in various orientations relative to the direction of gravity, it has to be

sufficiently stiff to preserve this static shear alignment during gimbal rotation. High stiffness is also needed to suppress vibrational shear that otherwise could be the cause of ghost contributions to the spectra.

GLORIA uses time-equidistant sampling with post processing to account for velocity variations (Brault, 1996). In the ideal case, this technique can cope with velocity variations approaching 100%. In reality, the optical paths of the infrared radiation and of the reference will not be completely identical and residual errors will arise. Based on unpublished experiences with MIPAS-STR, the goal for the velocity stability of the optical path difference measured by the reference laser system is 5% RMS which provides a reasonable trade-off between technical limitation and theoretical requirements.

In addition, the design of the spectrometer shall be compact and lightweight to allow its integration in the gimbal. Integrated local electronics are used on every gimbal frame as well as on the spectrometer itself in order to minimize the number of cables running through the gimbal axes. Furthermore, the pointing stabilization requires stiffness of the overall system – including the gimbal and the spectrometer – to enable pointing stability within 0.7 arcmin ( $1\sigma$ ) in elevation during the recording of an interferogram.

The mechanical systems have to cope with low environmental temperatures (down to 200 K) and pressure changes from 1000 hPa at ground to 70 hPa at flight altitude. Also vibrations impact the instrument and the spectrometer optics. The vibration requirements are driven by the performance of the interferometer. The design of the optics was specified to perform measurements during cruise flights with vibrations fitting two requirements. The first one defines that acceleration spectral peaks shall remain below 10% of the power spectral density (PSD) in DO 160C (Radio Technical Commission for Aeronautics (RTCA), 1989) “standard random vibration test curve for equipment installed in fixed wing aircraft with turbojet or turbofan engines, curve C”. This vibration limit is derived from measurements at different locations on the research aircraft Geophysica (MDB, 1996), where the envelope of the maximum PSD values are smaller than the 10% DO-160 curve. The second requirement concerns the overall root mean square acceleration  $G_{\text{rms}}$  which can be calculated by the square root of the integrated PSD curve. This value is given in the DO160C curve C with 4.12 g. The  $G_{\text{rms}}$  values during cruise are assumed to be below 10% of DO160C from experiences with MIPAS-STR on Geophysica and therefore smaller than  $4 \text{ m s}^{-2}$ . This corresponds to PSD values below 1% of DO160C.

These vibration values are given for the attachment points of the whole instrument at the carrier. However, these values are used as requirements for the spectrometer, too. In reality, the vibrations may be damped or increased by the structure of the gimbal. Additionally, vibrations can be caused by airflow.

Additional constraints are imposed by the flight certification process; static load strengths must be demonstrated by

**Table 1.** Mechanical and thermal requirements for the GLORIA spectrometer.

Interferometer	Optical path difference Velocity variation	$\pm 9$ cm < 5 % RMS
Detector module integration	Thermal input Integration concept	Shall be minimized Modular/demountable
Optics	Lens clear aperture Maximum field of view Environment	36.1 mm $4.1^\circ \times 4.1^\circ$ Dry and clean
Cooling system	Temperature Temperature drift	< 220 K < $2 \text{ K h}^{-1}$
Gimbal frame	Agility	Gimbal yaw $-20$ to $140^\circ$ Gimbal pitch $-98$ to $14^\circ$ Gimbal roll $0$ to $10^\circ$
Environmental conditions	Ambient temperature Ambient pressure Vibrations limits PSD during measurements Vibration limits $G_{\text{rms}}$ during measurements Max. humidity Housing surface	200 to 320 K 70–1000 hPa 10 % of DO160C curve C $4 \text{ m s}^{-2}$ (0.412 g) 100 % r. H. Dry
Static loads for strength	Forward HALO Forward Geophysica Up-/downward Side-/backward	2 g 9 g 3.2/6.3 g 3/1.5 g

calculations and testing. The requirements are different for HALO (Wernsdorfer and Witte, 2008) and for Geophysica (MDB, 2002). In Geophysica the instrument is inside of the fuselage and has to be handled as a built-in component. The choice of materials shall conform to aviation safety regulations.

The optical components have to be cooled below 220 K in order to sufficiently reduce the background thermal radiation and thus the background photon noise. The temperature should be spatially uniform in the optic module to avoid thermomechanical misalignment and disturbances due to air density fluctuations in the spectrometer. The temperature must also be temporally constant, with a drift rate smaller than  $2 \text{ K h}^{-1}$  to extend the time intervals between calibrations and to achieve a good radiometric accuracy (Kleinert et al., 2014).

For proper operation of the spectrometer in the harsh environment, care has to be taken to keep the cooled interferometer volume dry and clean. The outer surface should be kept free of condensate to reduce contamination and avoid disturbances at critical components such as on the entrance window or on electrical connectors. The requirements are summarized in Table 1.

The cooling system has to be located close to the interferometer optics – within the gimbal to avoid insulated or

pressurized hoses from one gimbal level to the other, which may impact the pointing stabilization performances. Compressor or Stirling coolers for the required working temperature and environment are bulky, heavy and generate vibrations. Their integration in the system is difficult. Therefore, a non-electrical cooling system with a reservoir of coolant was considered. It allows direct contact between the coolant reservoir and the interferometer on a large area and therefore enables good spatial temperature uniformity. The working duration should achieve at least 24 h to cover flights with two legs and short stopovers without maintenance. The pitch agility of the gimbal, covering  $112^\circ$ , makes the use of liquid coolants difficult.

Experiences from the precursor instruments MIPAS-B2 and MIPAS-STR have shown that operations during scientific measurement campaigns lead to additional requirements for the use of coolants: the coolant has to be refillable independently of the filling level or temperature of the instrument. This is required to handle delays in launch schedules. A coolant commonly available has to be chosen for operational considerations. The instrument's servicing ports have to be accessible through small hatches in the aircrafts fuselage to allow servicing without dismounting the cowling of the instrument bay. Finally, the capability to stabilize the temperature of the optic module during flight, on-ground and

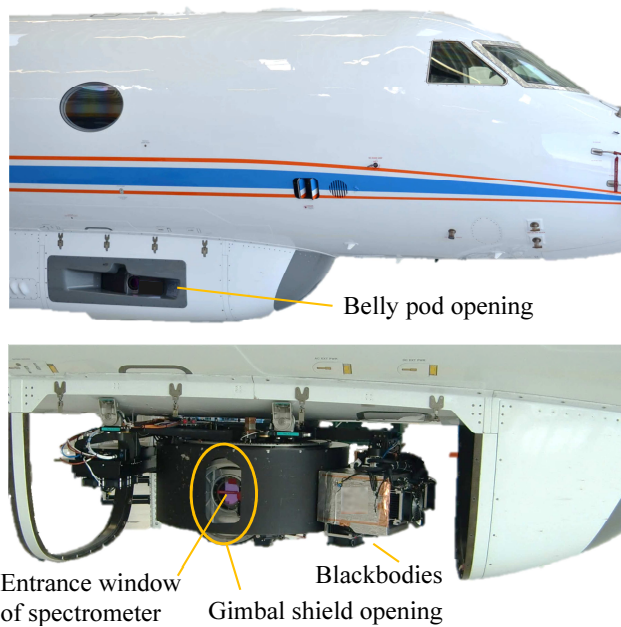


**Figure 1.** HALO with belly pod and opening for GLORIA (top) and belly pod with fairing dismounted showing the GLORIA instrument (bottom). The entrance window of the spectrometer is behind the opening in the gimbal's shield.

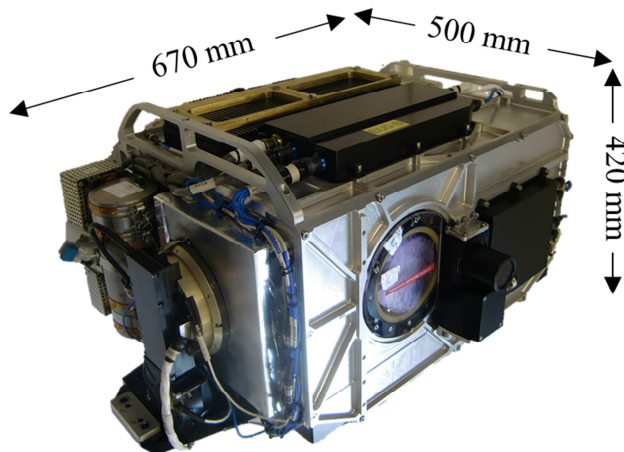


**Figure 2.** GLORIA Spectrometer ready for installation in the gimbal. Outer shell with electronic boxes (black), the entrance window (with cover), and the detector module (left side). The interferometer optics with cooling system is housed inside.

in the laboratory in a reproducible way is important for measurements and tests.

## 2.2 Overview

The GLORIA Instrument consists of the spectrometer in the three-axis gimbal, the blackbody calibration system, and the power electronics which are attached by a mounting frame to the hard-points in the fuselage of the aircraft by silicone

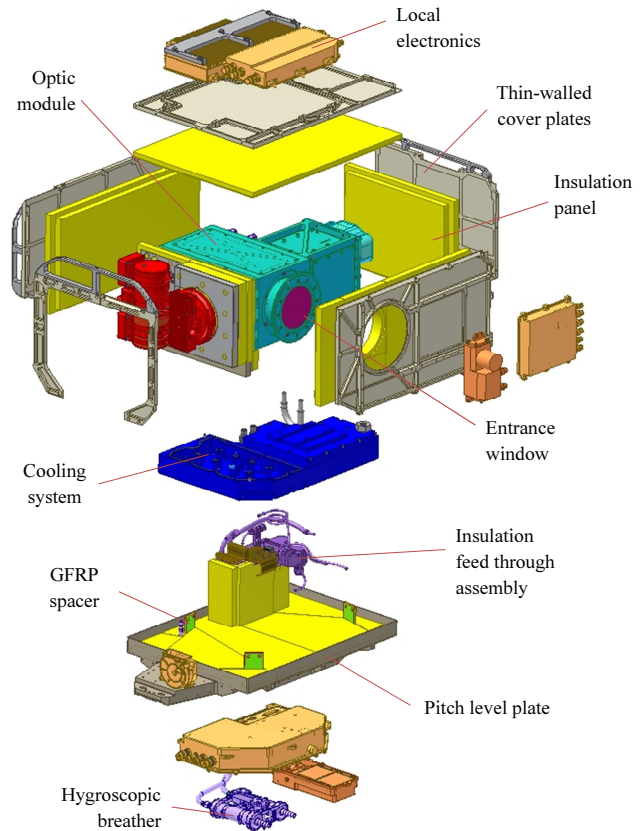


**Figure 3.** Exploded view of the GLORIA spectrometer showing components of the housing: pitch level plate, cover plates (grey), insulation (yellow), and local electronics (orange). Also shown is the optic module (cyan) with detector (red) and the cooling system (dark blue). External cables between electronic modules are not shown.

vibration isolators. The central control computer can be positioned in the cabin – for flights on HALO – or in the bay – for flights on Geophysica.

Figure 1 shows the GLORIA instrument on the HALO aircraft. The gimbal has a shield with an opening in front of the entrance window of the spectrometer. An elongated opening in the belly pod allows observation of the horizon with different gimbal yaw angles.

The spectrometer dismounted from the gimbal is shown in Fig. 2. The total mass of the spectrometer is 48 kg of which the cooled fraction is about 21 kg. The outer dimensions are 670 by 500 by 420 mm.

The spectrometer structure can be split into the three distinct parts shown in Fig. 3: the housing, the optic module, and the cooling system. The housing is built upon the gimbal pitch plate and forms, with additional cover plates, a protection shell containing the insulation. Both the cover plates and the gimbal pitch plate also serve as a support to electronic units. The optic module is a sealed compartment containing

all optical components, including the entrance window and the detector.

A cooling system based on dry ice has been chosen. Contamination of the interferometer volume with gaseous carbon dioxide has to be avoided because it is an atmospheric trace species measured by GLORIA. Therefore, the cooling system exhaust has to be diverted and the interferometer volume has to be properly sealed. For work in laboratories and during standby, an additional feedthrough with the possibility to inject cryogenic liquid nitrogen from a storage vessel for controlled cooling was added. This second coolant increases flexibility for ground operation. It is not suited for flights because the cooling system is not designed to store a liquid at 70 K.

Besides the cooling system, the use of vacuum insulation panels (VIP) is an important part of the thermal design. The highly efficient panels ensure low heat input and, therefore, allow a small coolant reservoir for the required holding time. With small insulation thickness due to the exceptionally low thermal conductivity, the volume required for the insulation is maintained small. The spatial temperature gradients in the optical system are reduced by using an all-aluminium structure with direct contact to the cooling tank and the use of the mentioned insulation. An insulation feedthrough assembly was designed to reduce local heat input along cables and cooling system tubes.

The entrance port for the incoming radiation breaks the thermal containment of the instrument. An assembly consisting of two air-spaced Germanium windows was preferred over a shutter system in order to meet the requirements in mass and size. This solution also enables the system to perform measurements in a humid environment at low altitudes or even on ground, supported by a heater for the outer entrance window to prevent condensation. Hygroscopic breathers allow pressure compensation between the closed cooled interferometer and the outside environment while protecting the optics from humidity and other contaminants.

The optical and electronic units are based on a modular design, which allows parallel maintenance of the subsystems and easy replacement during development or operation. It also facilitates improvement to specific subsystems. The reproducibility of the positioning for the optical components is ensured by dowel pin and hole or slot and key configurations. Electrical connections between interchangeable parts are realized by docking connectors.

Several PT1000 platinum resistance temperature sensors, four triaxial accelerometers, and two pressure sensors are mounted at key locations in and on the spectrometer. Together with the sensors on the gimbal and support structure, which also include a microphone, these sensors enable a detailed instrument characterization.

## 2.3 Housing

The base structure of the housing is the pitch level plate, working as a stiff chassis which holds further housings components as well as the optic module and the cooling system. The components are shown in Fig. 3. Both ends of the pitch level plate are mounted to the gimbals' pitch bearings and motor drive. The position of the pitch plate is such that the pitch rotation axis coincides with the spectrometer's center of gravity.

The housing cover consists of thin-walled plates with stiffening ribs machined out of high-strength aviation grade aluminium. The housing has only openings for the detector, for the entrance window, and for the insulation feedthrough assembly. The box protects the optic module and the VIP insulation.

The combined optic module and cooler are fixed to the pitch level plate by three glass-fibre reinforced plastic (GFRP) spacers. They allow a stiff connection while providing thermal insulation. A high degree of stiffness is important for this connection as it is critical for the line of sight stabilization performance. The position and orientation of the plates compensate different thermal expansion between optic module and pitch level plate.

### 2.3.1 Thermal insulation

The thermal insulation used to insulate the optic module and the coolant tank is based on VIP, which are made of evacuated micro porous fumed silicon dioxide (Fricke et al., 2006). The silicon dioxide core of the panels is sealed with a gas tight aluminized Polyester foil. Rectangular panels are arranged in two overlapping layers of a thickness of 10 to 15 mm around the optics. Triangle and edge cut panels are fitted around the GFRP spacers, the insulation feedthrough assembly and the entrance window. There are in total 38 individual panels forming a puzzle-like fitting. On the side panel where the detector is mounted, more flexible – although less effective – Polyethylene (PE) foam was preferred due to the large number of mechanical interfaces. The PE parts and the abutting faces of the VIPs are covered with aluminized Polyester tape to avoid convection and to protect the cold inner area from the infiltration of humidity and from the formation of condensate.

### 2.3.2 Insulation feedthrough assembly

The insulation feedthrough assembly, illustrated in Fig. 4 and shown with the cooling tank in Fig. 7, is the interfacing device between the cooled components and the outside environment. It provides a thermally insulated pass-through for all tubes and cables while minimizing heat input from outside to the cooler and optic module.

The insulation feedthrough assembly consists of two plates bonded together with a GFRP spacer tube. The warm-

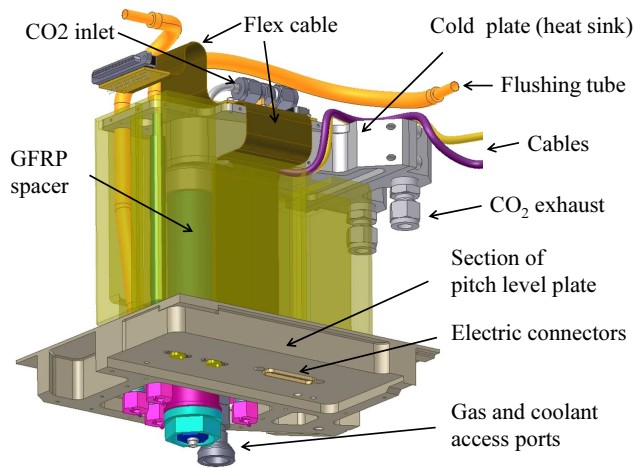


**Figure 4.** The insulation feedthrough assembly mounted on the pitch level plate (partly shown in gray). The heat input by tubes and cables between bottom part (ambient temperature) and top part (optic working temperature) is minimized.

end plate is fixed to the pitch level plate and the cold side plate acts as a heat sink cooled by the cold coolant gas exhaust. This design considerably reduces the heat load entering through the outer service connections. The tubes passing through the feedthrough include those for feeding coolant into the cooler system, purging exhaust gas and flushing various interior cavities.

The electrical feedthrough to the optic module consists of two cables and a custom designed combination of multilayer flex cable and printed circuit boards (PCBs). In the feedthrough, the cables pass around the cooler exhaust tube and the flex cable sideways down to the pitch level plate. At this location, MICRO-D electrical docking connectors, which are environmentally sealed, provide interface to the outer electronic modules. The intermediary PCB of the flex cable assembly is mounted on the heat sink to further reduce the heat load from outside introduced by the large number of copper wires. The whole feedthrough system is covered by an insulation foam housing and the internal hollow spaces are filled with styrofoam pellets to minimize convection.

### 2.3.3 Hygroscopic breathers

The spectrometer's internal spaces have to be pressure-balanced to the environment to avoid forces on the housing and the optic module. Two independent internal hollow spaces are found inside the spectrometer housing: the optic module free space and the open room between the housing and the optic module, including the interstices between insulation panels. Incoming air has to be dry and clean to protect the optics. Therefore, two hygroscopic breathers filled with molecular sieves and integrated particle filters are connected to the feedthrough assembly. This system allows ventilation, leaving a residual pressure difference of a few hPa

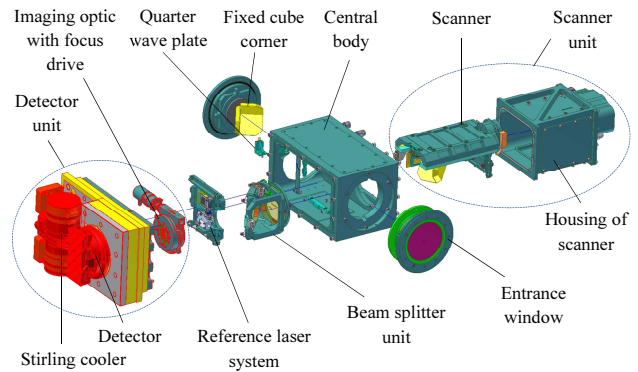


**Figure 5.** Exploded view of the optic module illustrating the main opto-mechanical (cyan) and optical components of the interferometer, the entrance window, the imaging optic and the detector system (red).

while limiting the input of humidity, CO<sub>2</sub> or other contaminants by adsorption. Servicing is done after about five flights by exchanging the filters and by regeneration of the molecular sieves.

## 2.4 Optic module

The optic module comprises of the entrance window assembly, the optical components of the Michelson interferometer, the imaging lens system, and the detector. The optic module also holds a reference laser system for measuring the optical path difference. The optic module is described in detail below in this section and shown in an exploded view in Fig. 5.

### 2.4.1 Central body and interferometer optics

The main structure of the optic module, the central body, is milled out of a massive block of fine-grained aluminium which exhibits low thermal distortions related to inner tension. The optic setup is modular and the subsystems are tightly mounted to the central body. The compact box-like platform makes the interferometer a system which shows high eigenfrequencies and is robust to external vibrations.

The optical components, along the path of the incoming radiation, are the entrance window assembly, the beam splitter unit (BSU), the fixed cube corner, the linear scanner with its moving cube corner, the adjustable infrared objective, and the detector. The supports and fixations for all optical components are made of the same aluminium alloy used for the central body, which leads to uniform thermal contraction during cooling and minimizes misalignments.

The infrared radiation enters the optic module via an insulating double window assembly which hermetically seals the central body. The diameters of the two AR-coated germanium optical windows are 100 mm whereas the optical beam at this location forms a rounded square with 78 mm sides. The plates are glued with silicone into two flanges held to-

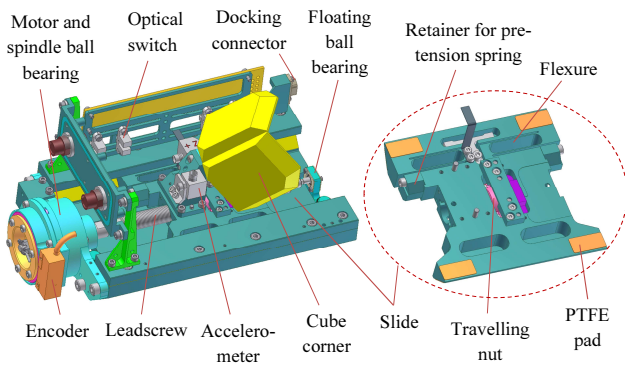


**Figure 6.** Complete scanner with slide (left) and detail of slide (right). The preloaded dovetail guidance with high contact area and a leadscrew for the feed motion was chosen to get a stiff and rigid design.

gether by a GFRP tube covered with aluminized Mylar foil to avoid diffusion of water vapor. The outer window can be heated to ensure operation above dew point, especially during ground operation and flight transitions at low altitudes.

The BSU consists (i) of a beam splitter with 104 mm diameter which is tilted  $45^\circ$  to the incoming beam and (ii) a separated compensation plate with 84 mm diameter which is oriented orthogonal to the reflected beam. Both, the wedged beam splitter substrate and the wedged compensation plate are made of KCl. The plates are fixed in a rigid aluminium structure by spring retainers.

The fixed cube corner is mounted onto the central body. In order to minimize shear errors, adjustment in the directions perpendicular to the incoming beam is necessary. The position of the fixed cube corner at operating temperature is determined through interferometric measurements. The cube corner positioning then can be reliably adjusted by the use of gauge blocks.

The custom made cube corners are gold-coated Zerodur facets fixed by contact bonding (Haisma and Spierings, 2002) with a clear aperture of 72 mm. An adapter is glued to the cube corner. It is made of Invar, which has a much lower thermal expansion coefficient than aluminium, and is therefore compatible with the use of Zerodur.

The reference laser is guided through the interferometer parallel to the infrared beam. It is folded from and back to the reference laser source and detection unit with folding mirrors above and below the imaging optic.

#### 2.4.2 Detector unit

The imaging optic is an air-spaced infrared achromat with a focal length of 72 mm at 218 K. It is mounted in a linear focusing stage in front of the detector. The stage allows movement of 4 mm in axial direction in order to adjust the position of the focal plane to compensate for fabrication tolerances and temperature-dependent focal length variations. The lin-

ear focusing stage is driven by a stepper motor with encoder. The torque is transferred by a worm drive and changed to a linear movement by a screw drive. The resulting high gear ratio of 148 turns to 1 mm linear movement of the objective, allows fine adjustment, and gives enough torque to operate in the specified temperature range.

The detector system, shown in red in Fig. 5, is a custom production by AIM, Heilbronn, Germany. It comprises of an FPA detector within a Dewar, the detector front-end electronics and a separate split Stirling cryogenic cooler connected by a helium transfer tube. Together with the imaging optic it forms the detector unit. The high-speed HgCdTe (mercury cadmium telluride) large focal plane array (LFPA) detector with 256 by 256 detector elements is sensitive in the mid and long-wave infrared spectral range between 7 and  $12.8\ \mu\text{m}$ . The spectral range is partly limited by the antireflection-coated germanium window of the Dewar. The detector is operated at a temperature of 50 K, which is maintained by the 4 W Stirling cooler. All detector unit components are mounted on a holding plate which is fixed to one long-side of the central body. The holding plate and the IR objective belong to the cooled space of the optic module whereas the detector itself and cooler are outside. Therefore, the detector Dewar and its front-end electronic as well as the compressor of the Stirling cooler are thermally insulated from the optic module and rigidly fixed by a GFRP-tube spacer and GFRP supports. Protection against electromagnetic interference is realized by conductive coating of the GFRP-tube, wrapping of the compressor in mu-metal and galvanic isolated mounting.

#### 2.4.3 Scanner

The opto-mechanical setup and especially the scanner has to endure the vibrations under the harsh environmental conditions during flight while holding true to the requirement for velocity variation under 5 % RMS.

The scanner assembly, shown in Fig. 6, was designed to maintain a stiff coupling between the moving cube corner and the central body. A rigid scanner construction was achieved with a base having high torsion and bending eigenfrequencies. For the guidance of the slide, a preloaded dovetail slide was chosen. Due to its large contact area, it is very stable and largely immune to external loads and vibrations when compared to ball-guided slides (Endemann, 1999) or guide slide bearings with small contact areas as used in high resolution laboratory spectrometers (Hase et al., 2013). These advantages are gained at the cost of higher friction; therefore, the material combination and lubrication have to be chosen carefully. For precise guidance of the slide in the dovetail, a lateral pretension is necessary, which is also important to compensate residual thermal expansion. The pretension is achieved by a flexure and supporting compression springs. This simple mechanical solution is flexible in one

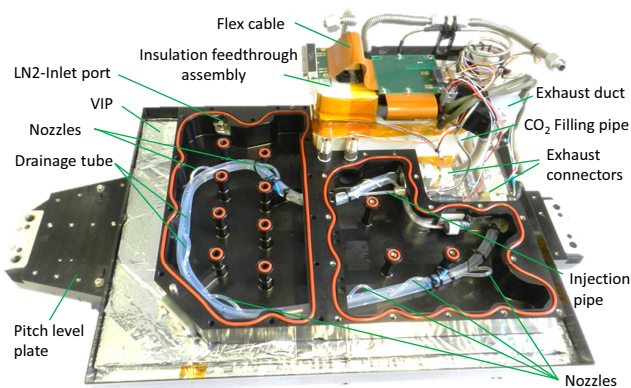


**Figure 7.** Coolant tank internal view with insulation feedthrough assembly (top right) mounted on the pitch level plate. The injection pipe is used to spray liquid CO<sub>2</sub> into the coolant tank through small nozzles. The liquid CO<sub>2</sub> is introduced over the feedthrough assembly into the tank. Precooling with LN<sub>2</sub> is possible over the dedicated LN<sub>2</sub> inlet. The exhaust gas is guided out by the drainage tube and heat sinking parts of the feedthrough.

direction while providing the necessary stiffness along the other directions.

Guidance and carriage are manufactured out of the same aluminium alloy used for all components of the optic module. The guiding surfaces are ground to get a good surface quality in terms of shape and roughness in order to provide a uniform movement with reduced friction. The surfaces are electroless nickel plated. Pads made out of polytetrafluoroethylene (PTFE) are used on the side of the carriage. The combination of PTFE with nickel leads to low friction with low slip-stick effect. The prefabricated parts were cryogenically cycled before finishing in order to reduce thermal distortion.

For the movement of the slide a leadscrew with 1 mm pitch is used. It provides a stiff coupling between the drive and the slide in the motion direction. The ground and polished leadscrew is made out of stainless steel. The traveling nut is made out of Polyimide with 15 % molybdenum disulphide (PI MoS<sub>2</sub> 15). The leadscrew is lubricated with lithium based grease, selected for low temperature operation. The leadscrew is supported with a pair of spindle bearings on the drive side and a roller bearing at the opposite end, acting as floating bearing, which are lubricated with perfluorinated polyether-based low temperature oil. A lightweight torque servo motor, the Robodrive ILM 50 × 14, is used as a direct drive. Rotor and stator are integrated to the leadscrew and motor housing respectively, leading to a lightweight and compact design. The rotation speed of the leadscrew is measured and controlled by an optical shaft encoder with 32 768 steps per revolution. The far end points are detected by optical switches. A nominal rotational velocity of 210 encoder steps per millisecond is preset which corresponds to a linear slide velocity of 6.41 mm s<sup>-1</sup>. Due to the factor of 2 between

the optical and the mechanical path difference, the optical velocity is twice the mechanical velocity.

## 2.5 Cooling system

In order to fulfil the thermal and logistical requirements described in Sect. 2.1 we decided to cool the optic module by a reservoir filled with dry ice. Charging solid CO<sub>2</sub> into a coolant tank (Piesch et al., 1996; Shallman and Shallmann, 2006; Pint and Thom, 2001) requires a large opening which disrupts the insulation. Additionally handling, deliverance, and storage of dry ice are costly. We have found a way to avoid these disadvantages by in situ production of dry ice in the coolant tank by expansion of liquid CO<sub>2</sub> (Büst, 2003, E.P. 1429093B1). With this method, it is possible to fill liquid CO<sub>2</sub> via a thin non-insulated flexible transfer tube and to store the coolant easily as pressurized CO<sub>2</sub> in gas cylinders. Carbon dioxide supplied in gas cylinders is commercially available. It is ideal for the application during campaigns even in remote areas as it has nearly unlimited storage time and poses little problem for transportation.

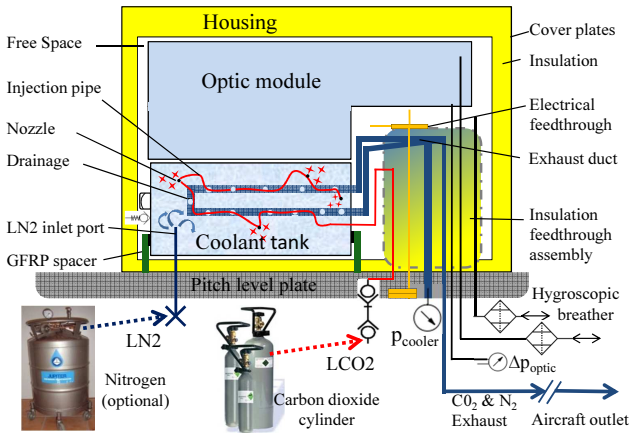
Cooling without dry-ice filling is also possible by injection of small amounts of liquid CO<sub>2</sub> into the tank. In addition, it is possible to use liquid Nitrogen sprayed inside the coolant tank at controlled intervals. In flight, the cooling system operates with dry ice, whereas liquid N<sub>2</sub> or CO<sub>2</sub> is destined for laboratory and ground operations.

Figure 7 shows the coolant tank construction. A small polyethylene pipe with holes in different zones of the coolant tank is used for filling carbon dioxide. The positions of the holes are optimized to fill the tank volume homogeneously with CO<sub>2</sub> snow. A constantan heating wire inside the injection polyethylene pipe protects blocking caused by freezing during the filling procedure. It also allows opening frozen sections of the pipe for the recharging process. A PTFE tube with larger diameter and perforated with holes drains the sublimation gas. The injection pipe and its integrated heating wire are guided and protected inside the PTFE drainage tube.

The small holes in the injection pipe act as spray nozzles and in these sections the polyethylene pipe is led outside the PTFE drainage tube. The injection pipe path and size, as well as the number of nozzles, their orientation and their opening have been empirically optimized in several tests to maximize the filled CO<sub>2</sub> snow mass.

The coolant tank has a total volume of 2.2 L and is machined out of a monolithic aluminium block by milling and spark-erosion. The coolant tank is designed for an overpressure of 10 bar to withstand the pressure forces exerted by the dry ice during filling and to operate the coolant tank at pressures up to 5 bar. The overpressure capability allows control of dry-ice temperatures from 173 K at 0.1 bar up to 216 K at 5 bar. The construction uses pillars to optimize the pressure resistance. The coolant tank is mounted directly below the optic module, which acts as cover for the tank; this configuration makes optimal use of conductive and convective cool-





**Figure 8.** Functional thermal setup of the GLORIA spectrometer. Injection of liquid CO<sub>2</sub> allows charging dry ice through in situ production of CO<sub>2</sub> snow in the coolant tank. Alternatively controlled cooling is possible by injecting small amounts of liquid CO<sub>2</sub> or liquid N<sub>2</sub>.

ing. The cooler is sealed by phenyl silicon O-rings (phenyl vinyl methyl quartz or PVMQ).

A separate inlet port on the bottom of the cooling tank enables access with an injection lance of a vacuum insulated transfer hose to spray liquid nitrogen in the tank. For safety reasons, two independent pressure relief valves and a bursting disc (not shown on Fig. 7) protect the cooler from overpressure.

## 2.6 Cooling operation

A functional schematic drawing which shows the GLORIA thermal setup and cooling system with its different cooling possibilities is shown in Fig. 8. During dry-ice filling or for controlled cooling, the exhaust port at the pitch level plate hose has to be fully open to release the exhaust gas. After dry-ice charging, a smaller hose leading to the aircraft outlet is connected to the main exhaust port.

### 2.6.1 Controlled cooling

Controlled cooling is achieved by dispersing liquid nitrogen or liquid carbon dioxide inside the coolant tank. The pressure drop and the evaporation of the liquid produce the desired cooling effect. This procedure can be used to cool down or to maintain the optic module at constant temperature. It is used in the laboratory or during ground operations while on campaign. The liquid nitrogen is taken out of cryogenic storage vessels by a siphon and is transferred to the LN<sub>2</sub> connector with a flexible vacuum insulated transfer line. Alternatively liquid CO<sub>2</sub> is taken out of standard CO<sub>2</sub> cylinders with riser pipe holding liquid CO<sub>2</sub> at room temperature and transferred to the LCO<sub>2</sub> connector. An external feedback loop controller, locked to a temperature sensor on the coolant tank, pilots

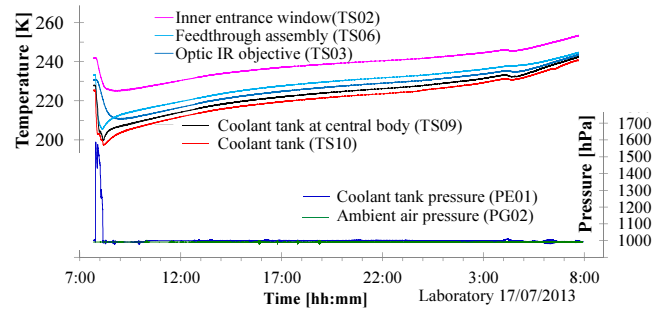


**Figure 9.** Spectrometer temperature and pressure values during laboratory testing of dry-ice filling (about 30 min) followed by laboratory operation without external coolant input.

a magnet valve on the transfer line, injecting an amount of coolant in the tank for controlled time periods. The injected coolant evaporates inside the cooling tank and the exhaust gas is guided out through the PTFE drainage tube.

### 2.6.2 Dry-ice cooling

The optic module is precooled before it is charged with dry ice. A custom built pressure regulator followed by a non-insulated transfer line provides the liquid CO<sub>2</sub> at 35 bar and slightly below room temperature to the LCO<sub>2</sub> connector. Inside the coolant tank, at the injectors, the CO<sub>2</sub> pressure drops to approximately 1.6 bar resulting in vaporization, which leads to the formation of dry ice as well as cold CO<sub>2</sub> gas. Evaporating CO<sub>2</sub> is drained out by the exhaust hose. The produced dry-ice snow has a temperature of about 195 K. Approximately 15 L of liquid CO<sub>2</sub> are sufficient to fill to the maximum capacity of 2.3 kg dry ice. Without the use of the injection pipe heater, the pipe and the nozzles freeze and get blocked before the coolant tank is filled at its nominal capacity. The whole filling procedure is monitored by observing temperature, pressure of the system, and the exhaust gas flow. The filling ends by itself when all nozzles are blocked by dry ice, which is clearly identifiable by a sudden drop of the exhaust flow and of the coolant tank internal pressure. At this point the fill valves are closed and the heating of the injection pipe is turned off.

Figure 9 shows the measurement of pressure and temperature during dry-ice filling and the following warming-up process. In this particular test, the spectrometer was not in operation and thus all internal heat sources were switched off, leaving only heat input through the housing. The pressure in the coolant tank rises up to 1600 hPa during filling of dry ice. It drops back to nearly ambient pressure after filling and stabilizes to a few hPa above ambient after connecting to the exhaust hose. The ambient temperature is about 294 K. Coolant tank charging needs less than 30 min whereby the temperature drops down to 200 K. The operational phase is characterized by increasing temperatures. This is caused by sublimation of the dry ice which reduces the contact area of

**Table 2.** Operational characteristics of the GLORIA cooling system.

Cooling system	Volume coolant tank	2.2 L
	Operating temperature (in flight)	200... 220 K
Controlled cooling (liquid)	Liquid CO <sub>2</sub> consumption	24 kg d <sup>-1</sup>
	Liquid N <sub>2</sub> consumption	9 kg d <sup>-1</sup>
	Liquid N <sub>2</sub> cooling to 220 K	3.5 kg
Charging dry ice	Filling time	30 min
	Fill quantity	2.3 kg
Dry ice cooling	Temperature drift (on ground)	1.6 K h <sup>-1</sup>
	Temperature drift (in flight)	1 K h <sup>-1</sup>
	Holding time	up to 24 h

**Table 3.** Heat load on the cooling system.

Insulation	In laboratory	17 W
Window	Heating included	3 W
Internal heat dissipaters	Scanner drive with encoder, focus drive of IR-imaging optic and reference laser system	5 W
Detector	With compressor	5 W

flow at the exhaust of the cooling system. Additionally, the result is verified by measuring the temperature drift without coolant. The distribution shown in Table 3 has been established with a series of laboratory measurements with different operation configurations.

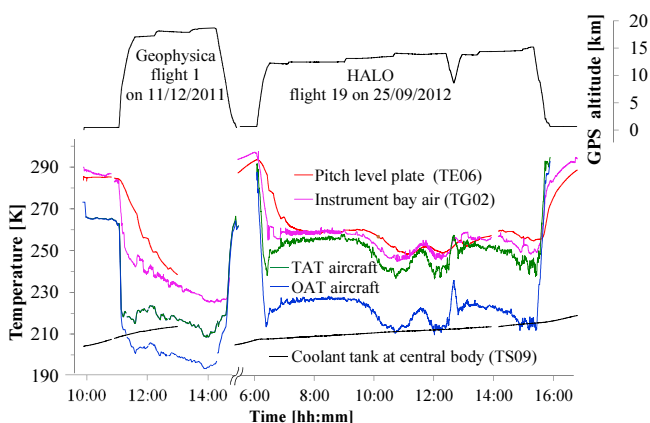
### 3 Results

#### 3.1 Environmental conditions

GLORIA has performed more than 100 flight hours on two different carriers. In this section results from three exemplary flights are presented: flight 1 on 11 December 2011 on the Geophysica in the polar winter and flights 8 and 19 on HALO at mid-latitudes on 28 August and on 25 September 2012.

Figure 10 shows temperature and altitude data of one flight with the Geophysica and one flight with HALO. The flight characteristics of both carriers differ in terms of altitude, duration, and velocity. The outside air temperature (OAT) during cruise varies from 190 to 230 K in function of the flight altitude and the meteorological conditions. Depending on the Mach number, the air flow at the aircraft warms up due to adiabatic compression; the so-called “ram rise” heating is about 17 K for Geophysica at Mach 0.66 and 28 K for HALO at Mach 0.81. The ram rise is included in the total air temperature (TAT). The air temperature measured in the Geophysica instrument bay reached 225 K (30 K above OAT) and in the HALO belly pod 253 K (33 K above OAT). The spectrometer housing with the pitch level plate is exposed to the ambient aircraft bay environment. During the first to second hour after takeoff, it cools down and stabilizes near the bay air temperature. The dry-ice cooled optic module operates at a temperature of about 210 K with a drift under 1 K h<sup>-1</sup> during the HALO flight. During the Geophysica flight, the drift was higher as the coolant tank was not charged to full capacity. The amount of coolant and the observed performances were sufficient for the typically short Geophysica flights. The optimized filling procedure with injection pipe heating and consequently a more complete fill level was later developed in preparation of the longer HALO flights.

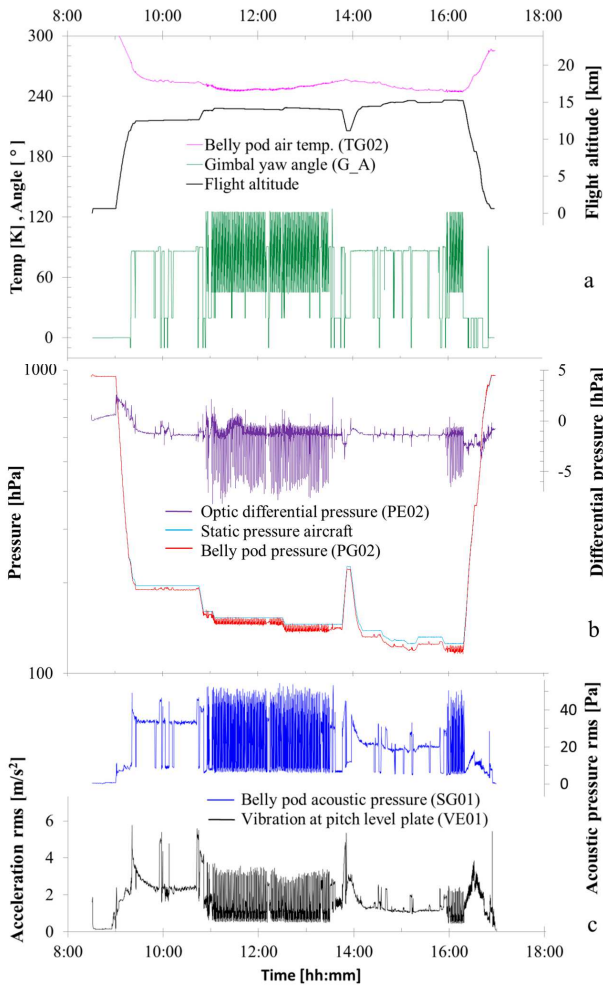
Figure 11 displays the conditions observed during flight 8. Figure 11a illustrates flight altitude, the gimbal yaw angle, and the belly pod air temperature. The gimbal coordinate system is relative to the aircraft orientation; the gimbal yaw an-



**Figure 10.** Ambient temperatures during typical operation of GLORIA on the Geophysica (left side) and HALO aircraft (right side). The evolution of ambient and instrument temperature is illustrated along flight altitude profile (OAT = temperature of undisturbed outside air, TAT = includes the hydrodynamic temperature rise caused by the airplane velocity).

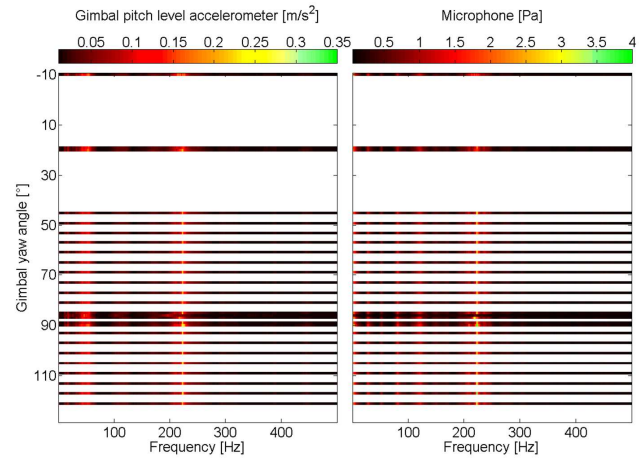
the coolant to the tank. Therefore a significant temperature drift of the optic module occurs, even when dry ice remains in the tank. This behavior is consistent with prior experience with coolers of MIPAS-B2 and MIPAS-STR which use latent heat from phase change of the coolant. The temperature increase rate depends on the coolant tank geometry, the heat load, and the different thermal conductivity of the coolant’s phases; the CO<sub>2</sub> gas has a 20 times lower thermal conductivity than dry ice. Figure 9 shows a relatively constant temperature drift, rising from 200 to 230 K in 19 h while dry ice remains in the coolant tank. During flight the observed temperature drifts are smaller due to a lower heat load related to the lower environmental temperature (see Sect. 3.3).

Table 2 summarizes the operational characteristics of the GLORIA cooling system for both liquid N<sub>2</sub> and liquid CO<sub>2</sub> cooling, including holding time and consumption. Table 3 shows the occurring heat loads. The total heat load is calculated based on the measured coolant weight and the gas



**Figure 11.** Ambient conditions of GLORIA during flight 8 on HALO on 28 August 2012: (a) belly pod air temperature (pink), flight altitude (black), and gimbal yaw angle (green), (b) optic differential pressure (purple), static pressure aircraft (light blue), and belly pod pressure (red), and (c) belly pod acoustic pressure (blue) and spectrometer vibrations (black).

gle is varied during operation between  $-10$  to  $128^\circ$ , where at  $0^\circ$  the entrance window is pointing along the aircraft longitudinal axis. At  $-10$  and  $20^\circ$  yaw angles, the window is respectively aligned with the cold and the warm blackbody for radiometric calibration. The CM measurements are carried out at around  $86^\circ$  gimbal yaw angle. During the DM measurements, which were performed between 11:00 to 13:30 UTC and between 16:00 to 16:20 UTC as shown in Fig. 11, the gimbal yaw angle changed rapidly: the yaw angle is varied every 3 s in  $4^\circ$  steps from  $128$  to  $44^\circ$  yaw angle to scan the horizon. This measurement mode can be clearly recognized by the variation of the gimbal yaw angle in Fig. 11a. The atmospheric measurements are periodically interrupted for internal calibration.



**Figure 12.** Spectrogram of vibration and acoustic pressure measurements of the pitch level plate for different gimbal yaw angles averaged over the whole flight 8 on HALO on 28 August 2012. Only discrete gimbal yaw angles are illustrated, as only those angles are used during the measurements.

Figure 11b shows the outside static air pressure given by aircraft measurements, which goes down to 130 hPa. The pressure inside the belly pod generally follows the outside pressure with a slight fluctuation correlated with the gimbal yaw angle due to air streaming through the side opening. The differential pressure measurement shows the pressure difference between the inside of the optic module and the belly pod. The pressure fluctuations in the belly pod can also be seen in this differential pressure, causing variations down to  $-8$  hPa. The plot also depicts the pressure variations caused by the breathing of the instrument during ascent, descent, and dives in the range of  $\pm 2$  hPa. This is caused by flow resistance through the hygroscopic breathers.

Figure 11c presents the acoustic pressure in the belly pod and the vibrations measured at the pitch level plate. Shown are the RMS values for time periods of 1.2 s during DM measurements and 12 s during CM, respectively. Beside an obvious and expected correlation between the values and the gimbal yaw angle, the mean of these values depend clearly on the flight level. For lower cruise altitudes of 12.6 km at 10:30 UTC the acceleration mean level is about  $2.3 \text{ ms}^{-2}$  and goes down to  $1.1 \text{ ms}^{-2}$  at 15 km height at 15:00 UTC. The behavior of the acoustic pressure is similar. The dependency of the vibrations on the gimbal yaw angle, as well as on the flight altitude, and therefore air density, is explained by aerodynamic forces caused by the belly pod opening.

Figure 12 shows the spectrograms of the vibrations measured at the pitch level plate – the base of the spectrometer – and the acoustic pressure in the belly pod. The sampling rate of the sensors is 1 kHz. In addition to Fig. 11c, these plots depict the spectral contributions for different gimbal yaw angles. The microphone as well as the accelerometer clearly show the strongest vibration amplitudes between 200

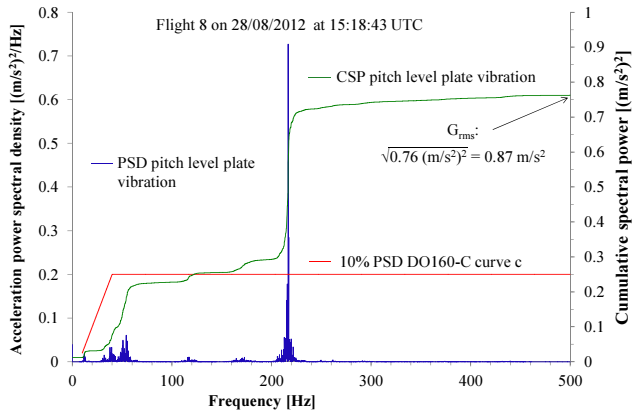


**Figure 13.** Vibration measurement at pitch level plate during flight 8 on HALO during chemistry mode measurement at gimbal yaw angle of approximately  $86^\circ$ . Shown are the measured power spectral density (PSD) (blue) and its cumulated spectral power (CSP) (green) as well as the PSD of the assumed limit of 10 % DO-160C curve c (red) for single vibration peaks.

and 250 Hz throughout the whole flight. This excitation probably originates aerodynamically at the belly pod side opening and appears at all gimbal yaw angles with varying amplitude. The highest value occurs at a gimbal yaw angle of  $90^\circ$ . Analysis of different sensor data indicates that the aerodynamic excitation changes with the position of the gimbal's shield and its opening relative to the airflow.

In order to avoid the strong vibrations at  $90^\circ$ , the CM measurements have been performed at a yaw angle of  $86\text{--}87^\circ$ . Another clearly visible frequency band at 40–60 Hz in the accelerometer data is related to resonant frequencies of the gimbal and its shield. All other visible bands in both plots have considerably smaller amplitude.

### 3.2 Mechanical performance

A key indicator of the spectrometer function quality is the measurement of the moving mirror velocity using the reference laser system (Learner et al., 1996; Kimmig, 2001). It gives a good insight on the stiffness and damping characteristics of the system and on the impact of the vibrations on the IR measurement. The velocity measured with the reference laser system is directly proportional to the velocity of the moving cube corner and should ideally be constant. Unwanted velocity fluctuations are generated by fluctuations in the cube corner movement, but also by relative movements of the optical parts to each other. Such relative movements can e.g., be caused by independent vibrations of the optical components and the structure.

In order to quantify the stiffness of the spectrometer the inflight vibrations and the effects to the reference signal velocity are shown in Figs. 13 and 14. These pictures show the vibrations on the pitch level plate and the velocity signal recorded by the reference laser system over one interfer-

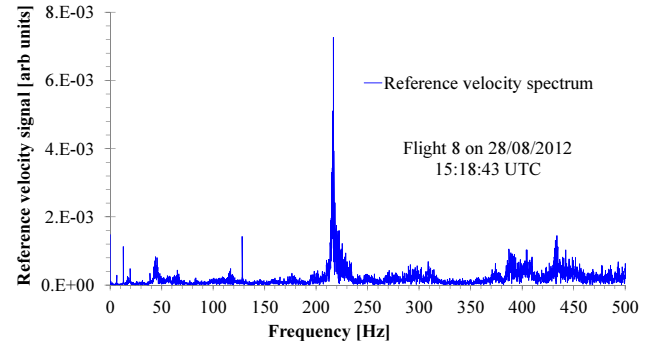


**Figure 14.** Spectrum of the velocity signal from the interferometer measured with the reference laser during the same time period which is illustrated in Fig. 13. The largest peak is caused by the strongest vibration identified in Fig. 13.

ogram at 15:18 UTC during flight 8 while the spectrometer is operated in CM. The environmental conditions remained stable at the time as shown in Fig. 11 in the previous section. The gimbal yaw angle varied only slightly in the range of  $86.0$  to  $86.6^\circ$  and the altitude was close to 15 km.

Figure 13 shows the power spectral density (PSD) of the vibration magnitude in the direction of scanner motion measured on the pitch level plate. This plot is derived from a single spectrum. Furthermore the integrated value of the PSD, the cumulative spectral power (CSP), is displayed. The peaks in the PSD and steps in the CSP curve show very clearly that the largest power contribution of the vibrations is found around 50 and 220 Hz. The red curve shows the PSD limit for single vibration peaks in operational conditions as described in Sect. 2.1 and summarized in Table 1. It can be noted that the excitation at 217 Hz exceeds this requirement. The integral of the vibration excitation, the so-called root mean square acceleration  $G_{\text{rms}}$ , can be derived out of the CSP to  $0.87 \text{ m s}^{-2}$ . This is lower than the requirement which was set to  $4 \text{ m s}^{-2}$ .

The velocity signal detected by the reference laser for the same time interval shows a standard deviation of 9 %, exceeding the target value of 5 % given in Table 1. Figure 14 shows the amplitude spectrum of the velocity. The largest contribution to the velocity fluctuations is again around 217 Hz in accordance with the measured vibrations. Furthermore, there are sharp peaks which are found at multiples of 6.41 Hz. They are caused by the leadscrew of the scanner which has a rotation rate of 6.41 Hz. The second largest peak, which can be found at 128.2 Hz, is generated by the cogging torque of the twenty electrical coils in the stator of the drive.

The main part of the velocity fluctuations in the interferometer is caused by forced vibrations of the optical components induced by the strong acoustic and mechanical excitations around 220 Hz as shown in Fig. 12. The strong velocity variations around 220 Hz lead to so-called “ghost”-signatures in the spectra (Learner et al., 1996; Kimmig,

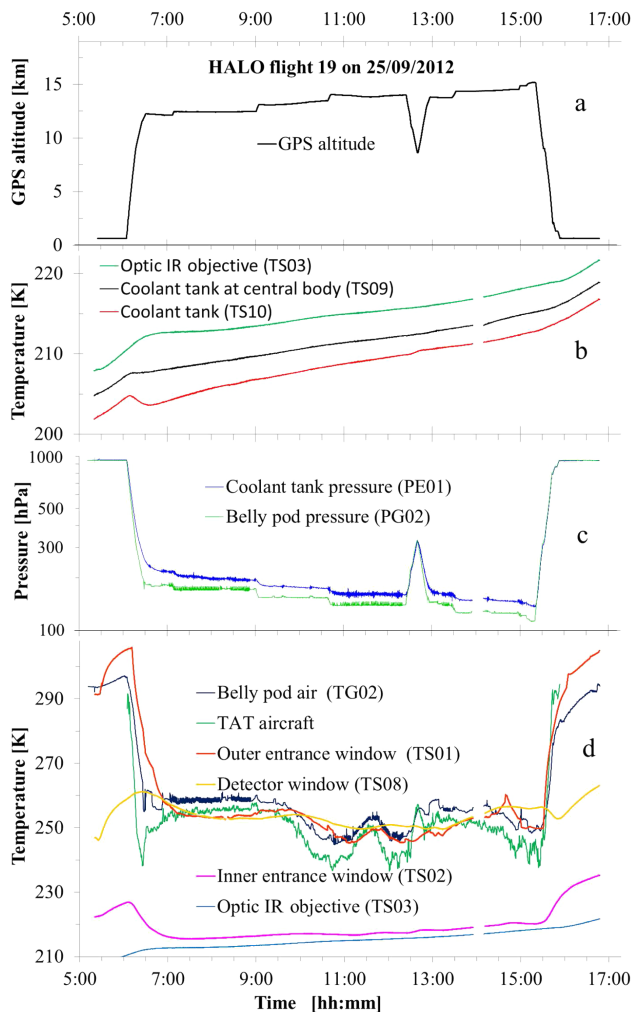


**Figure 15.** Conditions observed during flight 19 on HALO. The plots show (a) flight altitude, (b) optic and coolant tank temperatures, (c) coolant tank pressure, (d) aircraft and window temperatures.

2001). The frequency distribution of the velocity variations is broad in comparison to individual lines, leading to a smearing of ghost lines, which makes them indiscernible from noise. Only broad band signatures like the ozone band produce visible ghost patterns. A ghost amplitude of 1–2 % is estimated from these broad patterns. Spectral regions contaminated with these broad band signatures are used with great care in the retrieval of atmospheric parameters. A precise quantification of the impact on temperature and trace gas profiles has not been performed yet.

### 3.3 Thermal performance

The temperatures measured inside and outside the spectrometer and the flight altitude are shown in Fig. 15 for flight 19 on the HALO aircraft. The same flight was already discussed in Sect. 3.1. In Fig. 15b the temperatures inside the optic

module and the coolant tank are shown. The sensor on the coolant tank, identified as “coolant tank” is the farthest away from the central body and shows the lowest temperature of the cooling system. The sensor “coolant tank at central body” is located at the interface between the central body and the coolant tank. It shows the highest temperature of the cooling system and the lowest temperature of the central block as expected. A third sensor, positioned in the IR objective, shows the highest measured temperatures inside the optic module with the exception of the entrance and detector windows. The temperature of the latter is influenced by the environmental pressure, window heating and indirect heating by electronic components. Both window temperatures are shown in Fig. 15d.

The cooler had been filled with dry ice approximately 2 h before takeoff. During flight preparation, visualized as a constant GPS height near 0 m in Fig. 15a, the coolant tank warmed up rapidly with about  $4 \text{ K h}^{-1}$ . During ascent, the coolant tank temperature drops again due to the ambient pressure decrease. In this flight phase, the increase rate of the optic module temperature becomes smaller before stabilizing at the typical inflight increase rate of approximately  $1 \text{ K h}^{-1}$ .

The inflight temperature of the optic module remains below 220 K. The temperature difference between the coldest and warmest components in the optic module is below 4 K while the coolant tank is at most 3 K colder than the optic module.

The belly pod and the cooling system pressure are shown in Fig. 15c. The pressure in the unpressurized coolant tank follows the aircrafts ambient pressure. Due to pressure decrease with increasing altitude the sublimation temperature of the dry ice drops. This leads to a higher sublimation rate and thus to a higher overpressure of 50 hPa. The overpressure diminished to approximately 22 hPa during flight. The higher overpressure observed in the cooling tank during flight compared to ground operation is also caused by the reduced gas density at flight level requiring a higher volume for the same mass flow of  $\text{CO}_2$ .

The temperature drifts of the entrance and detector windows are required to be below  $2 \text{ K h}^{-1}$ , as for all optical components. For the windows, this requirement is technically challenging due to the exposed position at the boundary of the cold system with unavoidable gaps in the thermal insulation. As depicted in Fig. 15d, temperatures of outer and inner windows of the entrance window assembly are strongly influenced by the aircraft environment. The outer window is also strongly affected by its heating system which is needed to prevent condensation. The temperature gradient inside the entrance window assembly is approximately 35 K inflight without heating and 80 K on ground while heating.

The inner window temperature drift is with  $1 \text{ K h}^{-1}$  similar to the other optical components and thus in accordance with the requirements. Stronger temperature drifts can be observed while the outer window heater is operating. These

drifts do not affect the performance of the system as no scientific measurements are taken while the heater is active.

The outer window temperature is strongly affected by the environmental conditions and the outside airflow. This leads to temperature drifts that exceed the requirements. For instance between 10:00 and 11:00 UTC a drift of  $-10 \text{ K h}^{-1}$  is observed correlated with the belly pod temperature. This seems to indicate an atmospheric condition change. Other sudden changes in the outer window temperature exceeding  $10 \text{ K h}^{-1}$  can also be observed. These are mostly correlated with the gimbals yaw angle changes, indicating an influence of the outer air flow around the window.

The detector window temperature shown in Fig. 15d varies smoothly without sudden changes during flight. The drift of  $5 \text{ K h}^{-1}$  is significantly smaller than for the outer entrance window but still exceeds the requirement.

#### 4 Conclusions and outlook

Remote sensing of atmospheric trace constituents with high spectral and spatial resolution requires a compact and rigid interferometer with permanently cooled optics. The chosen design of the instrument led to the successful operation on two different research aircrafts in unpressurized compartments under harsh and variable ambient conditions.

Especially the scanner with linear dovetail slide contributed to achieve a rigid optical system. The dove-tail slide suppresses relative motion of the cube corner and its guidance induced by external vibrations.

As the emission of the trace constituents is only measurable with cooled optics, we designed a cooling system mounted directly to the optic module. It is based on dry ice injected as liquid carbon dioxide. Alternatively, the cooling system also works with liquid nitrogen. The application of vacuum insulation panels contributed to the compact design. The cooling system and the insulation feedthrough assembly enable operability of the instrument in a wide range of ambient temperature and humidity while the dry ice capacity ensures a hold time of 24 h. Inflight measurements show that the thermal requirements could be fulfilled as the temperature drift could be kept below  $1 \text{ K h}^{-1}$  for most of the optical components at an operating temperature below 220 K.

The use of liquid  $\text{CO}_2$ , a non-cryogenic product commercially and widely available in gas cylinders with unlimited holding time makes the instrument suitable for campaigns all over the world. Filling the coolant at ambient temperature allows using an uninsulated hose and therefore easy access through small hatches. It is conceivable to use the developed cooling techniques for any type of instrument, devices or calibration sources with similar thermal specifications.

Since the first scientific campaigns with GLORIA were successful, GLORIA will further participate in dedicated campaigns in 2016 and the years following (Riese et al., 2014). For future flights, the vibration analysis presented in Sec. 3.2 has resulted in modification plans for the HALO

belly pod, e.g., a spoiler in front of the opening. Additional changes to the gimbal's shield in order to reduce the aerodynamical excitation and to increase the stiffness of the gimbal are carried out. The central body and the housing of the scanner will be replaced by a monolithic housing to increase the stiffness of the optic module and to reduce the influences of the vibrations. Further improvements concentrate on the thermal fluctuations of the entrance and the detector window. Different strategies, e.g., changing the design of the detector unit to improve the insulation using VIP, integrating a cooling shield around the detector dewar to stabilize the window temperature, and an enhanced strategy to consider the entrance window temperature during calibration are currently being investigated.

*Acknowledgements.* We would like to thank the head of the prototyping facility at KIT IMK-ASF, A. Streili, for his commitment during the development of the GLORIA spectrometer. We thank the whole DLR flight operations team at Oberpfaffenhofen for the excellent flights. We are grateful to the DLR certification team for their valuable cooperation and support during testing and certification. We acknowledge the close collaboration with our partners at MDB, which has allowed the unique operation of our spectrometers in the lower stratosphere. The excellent infrastructure at Kiruna airport and the uncomplicated support by the airport staff have made Kiruna an unrivaled campaign site for us.

We acknowledge support by the Deutsche Forschungsgemeinschaft and Open Access Publishing Fund of the Karlsruhe Institute of Technology.

The article processing charges for this open-access publication were covered by a Research Centre of the Helmholtz Association.

Edited by: J. Notholt

#### References

- Brault, J. W.: New approach to high-precision Fourier transform spectrometer design, *Appl. Optics*, 35, 2891–2896, doi:10.1364/AO.35.002891, 1996.
- Brasunas, J. C., Kunde, V. G., and Herath, L. W.: Cryogenic Fourier spectrometer for measuring trace species in the lower stratosphere, *Appl. Optics*, 27, 4964–4976, 1988.
- Büst, W.: Versorgung einer Einrichtung zur Temperaturhaltung mit Kohlendioxidschnee, *Europäische Patentschrift EP 1 429 093B1*, 2003.
- Carli, B., Barbis, A., Harries, J. E., and Palchetti, L.: Design of an efficient broadband far-infrared Fourier-transform spectrometer, *Appl. Optics*, 38, 3945–3950, 1999.
- Endemann, M.: MIPAS instrument concept and performance, in: *European Symposium on Atmospheric Measurements from Space*, Noordwijk, the Netherlands, 1999.
- Fricke, J., Schwab, H., and Heinemann, U.: Vacuum insulation panels – exciting thermal properties and most challenging applica-

- tions, *Int. J. Thermophys.*, 27, 1123–1139, doi:10.1007/s10765-006-0106-6, 2006.
- Friedl-Vallon, F., Maucher, G., Seefeldner, M., Trieschmann, O., Kleinert, A., Lengel, A., Keim, C., Oelhaf, H., and Fischer, H.: Design and characterization of the balloon-borne Michelson Interferometer for Passive Atmospheric Sounding (MIPAS-B2), *Appl. Optics*, 43, 3335–3355, 2004.
- Friedl-Vallon, F., Gulde, T., Hase, F., Kleinert, A., Kulesa, T., Maucher, G., Neubert, T., Olschewski, F., Piesch, C., Preusse, P., Rongen, H., Sartorius, C., Schneider, H., Schönfeld, A., Tan, V., Bayer, N., Blank, J., Dapp, R., Ebersoldt, A., Fischer, H., Graf, F., Guggenmoser, T., Höpfner, M., Kaufmann, M., Kretschmer, E., Latzko, T., Nordmeyer, H., Oelhaf, H., Orphal, J., Riese, M., Schardt, G., Schillings, J., Sha, M. K., Suminska-Ebersoldt, O., and Ungermann, J.: Instrument concept of the imaging Fourier transform spectrometer GLORIA, *Atmos. Meas. Tech. Discuss.*, 7, 2301–2337, doi:10.5194/amtd-7-2301-2014, 2014.
- Haisma, J. and Spierings, G. A. C. M.: Contact bonding, including direct-bonding in historical and recent context of material science and technology, physics and chemistry, *Mat. Sci. Eng. R.*, 37, 1–60, 2002.
- Hase, F., Drouin, B. J., Roehl, C. M., Toon, G. C., Wennberg, P. O., Wunch, D., Blumenstock, T., Desmet, F., Feist, D. G., Heikkinen, P., De Mazière, M., Rettinger, M., Robinson, J., Schneider, M., Sherlock, V., Sussmann, R., Té, Y., Warneke, T., and Weinzierl, C.: Calibration of sealed HCl cells used for TCCON instrumental line shape monitoring, *Atmos. Meas. Tech.*, 6, 3527–3537, doi:10.5194/amt-6-3527-2013, 2013.
- Kimmig, W.: Das Abtastverfahren der Interferogramme des flugzeuggetragenen Fourierspektrometers MIPAS-STR, *Wissenschaftliche Berichte FZKA*, 6665, Dissertation, Universität Karlsruhe, 2001.
- Kleinert, A., Friedl-Vallon, F., Guggenmoser, T., Höpfner, M., Neubert, T., Ribalda, R., Sha, M. K., Ungermann, J., Blank, J., Ebersoldt, A., Kretschmer, E., Latzko, T., Oelhaf, H., Olschewski, F., and Preusse, P.: Level 0 to 1 processing of the imaging Fourier transform spectrometer GLORIA: generation of radiometrically and spectrally calibrated spectra, *Atmos. Meas. Tech. Discuss.*, 7, 2827–2878, doi:10.5194/amtd-7-2827-2014, 2014.
- Krautstrunk, M. and Giez, A.: The transition from FALCON to HALO era airborne atmospheric research, in: *Atmospheric Physics, Research Topics in Aerospace*, Springer-Verlag, Heidelberg, Germany, 609–624, doi:10.1007/978-3-642-30183-4\_37, 2012.
- Kullmann, A., Riese, M., Olschewski, F., Stroh, F., and Grossmann, K. U.: Cryogenic infrared spectrometers and telescopes for the atmosphere – new frontiers, *P. SPIE*, 5570, 423–432, 2004.
- Learner, R. C. M., Thorne, A. P., and Brault, J. W.: Ghosts and artifacts in Fourier-transform spectrometry, *Appl. Optics*, 35, 2947–2954, 1996.
- MDB: Po opredeleniju vibronaprjaženosti blokov apparatury i mest ih ustanovki, Determination of the vibration load of the instruments and their installation locations, Myasishchev Design Bureau, Moscow, Russia, 1996.
- MDB: High-altitude M55 Geophysica aircraft, Investigator Handbook, 2nd Edn., Myasishchev Design Bureau, Moscow, Russia, 2002.
- Olschewski, F., Ebersoldt, A., Friedl-Vallon, F., Gutschwager, B., Hollandt, J., Kleinert, A., Monte, C., Piesch, C., Preusse, P., Rolf, C., Steffens, P., and Koppmann, R.: The in-flight blackbody calibration system for the GLORIA interferometer on board an airborne research platform, *Atmos. Meas. Tech.*, 6, 3067–3082, doi:10.5194/amt-6-3067-2013, 2013.
- Piesch, C., Gulde, T., Sartorius, C., Friedl-Vallon, F., Seefeldner, M., Wölfel, M., Blom, C. E., and Fischer, H.: Design of a MIPAS instrument for high-altitude aircraft, in: *Proc. of the 2nd Internat. Airborne Remote Sensing Conference and Exhibition, ERIM, Vol. II*, Ann Arbor, MI, 199–208, 1996.
- Pint, K. R. and Thom, W. F.: Dry Ice Cooler, United States Patent US 6212901B1, Alexandria, VA, USA, uspto, 2001.
- Riese, M., Oelhaf, H., Preusse, P., Blank, J., Ern, M., Friedl-Vallon, F., Fischer, H., Guggenmoser, T., Höpfner, M., Hoor, P., Kaufmann, M., Orphal, J., Plöger, F., Spang, R., Suminska-Ebersoldt, O., Ungermann, J., Vogel, B., and Woiwode, W.: Gimballed Limb Observer for Radiance Imaging of the Atmosphere (GLORIA) scientific objectives, *Atmos. Meas. Tech. Discuss.*, 7, 1535–1572, doi:10.5194/amtd-7-1535-2014, 2014.
- RTCA DO-160C: Environmental conditions and test procedures for airborne equipment, Washington, RTCA, 1989.
- Shallman, R. W. and Shallmann, E. C.: Low temperature cooler, United States Patent, US 2006/0053828 A1, 2006.
- Wernsdorfer, T. and Witte, K.: Technical Note HALO-TN-2007-003-B, Rev. B, DLR, Oberpfaffenhofen, 2008.